Journal of Control, Automation and Electrical Systems (2021) 32:245–255
https://doi.org/10.1007/s40313-020-00669-7

LPV/$\mathcal{H}_\infty$ Control of a Twin Hull-Based Unmanned Surface Vehicle

Eduardo S. Rodriguez-Canales[1] · **Juan C. Cutipa-Luque**[1]

Received: 19 December 2019 / Revised: 8 September 2020 / Accepted: 10 November 2020 / Published online: 3 January 2021

Abstract
This work presents a robust control system for a twin hull-based unmanned surface vehicle, named EDSON-J, which is being built at the *Universidad Nacional de San Agustín de Arequipa* and whose main mission is the autonomous monitoring of ocean water quality and lagoons vulnerable to heavy metal contamination. The vehicle has been designed to carry additional payload consisting of electronic instrumentation destined to measure the water conditions in real time. This paper focuses on the control design of controllers for an unmanned surface vehicle with mass as parameter varying. The approach used is the linear parameter-varying control (LPV control); its goal is to synthesize a controller that guarantees robust stability and performance of the system despite the presence of parameter varying, disturbances and sensor noise. The simulation results, in frequency domain and time domain, show an improvement in the LPV robust control approach in comparison with LTI/$\mathcal{H}_\infty$ controllers.

Keywords Linear parameter varying (LPV) · Robust control · Unmanned surface vehicle (USV) · Maneuvering model

1 Introduction

The development of maritime vehicles is essential in missions of supervision of biological resources, environment, maritime cartography and national security. The periodic use of manned vessels is unfeasible due to its high cost of operation and the maintenance of the crew. The unmanned surface vehicle (USV) is a better alternative for maritime operations due to its low operating cost, in addition to its greater autonomy and payload capacity with respect to air and submersible vehicles, being able to even serve as a mobile control station for them.

In the last decades, several projects of autonomous maritime vehicles have been developed for research, industry and military applications. In 1993, the MIT began a development project of autonomous vehicle named ARTEMIS (Manley 2008), a vehicle which consists of two modified kayaks commanded with conventional proportional derivative control system. In 2000, after a series of improvements in navigation, guidance and control systems, the vehicle was renamed AutoCat (Manley et al. 2000). In 2006, the DELFIM USV (Alves et al. 2006) was developed by the University of Lisbon to acquire marine data and to serve as a relay between submerged craft and vessels. The USV has an integration of guidance and control systems based on path following and trajectory tracking approaches. Charlie (Caccia et al. 2007) is another USV that has a real-time operative system (RTOS) based on GNU/Linux, a line of sight (LOS) guidance system and a control system based on proportional derivative heading control. The ROAZ II USV (Martins et al. 2007) was developed for search and rescue missions and has a system for identifying objectives and orientation based on robotic vision. In 2013, the HTWG Konstanz developed the CaRoLime USV (Wirtensohn et al. 2013) for missions of limnology in rivers and inland waters. Its dynamic model was identified via least square optimization approach and using a swarm optimization algorithm achieving good matching results between the simulation and the experimental tests.

Linear and nonlinear robust control approaches aim mainly to ensure the stability and performance of the maritime vehicles subject to perturbations. The advanced control approaches have been explored and implemented in many

This document is the result of the research project funded by the Universidad Nacional de San Agustín de Arequipa, with Grant IBAIB-08-2018-UNSA.

✉ Eduardo S. Rodriguez-Canales
erodriguezca@unsa.edu.pe

Juan C. Cutipa-Luque
jcutipalu@unsa.edu.pe

[1] Graduate Program in Electronic Engineering of Universidad Nacional de San Agustín de Arequipa (UNSA), Calle Santa Catalina 117, Arequipa, Arequipa, Peru

maritime vehicles to overcome the problem of robustness and good performance despite unmodeled dynamics, uncertainties, external disturbances and noise in inertial navigation sensors. For example, a centralized $\mathcal{H}_\infty$ robust control approach with two-degree-of-freedom (TDOF) structure was developed for controlling an autonomous underwater vehicle (AUV) (Luque and Donha 2008). Robustness in stability and good performance are achieved for the multivariable dynamics of the AUV, validated both numerically and experimentally (Cutipa-Luque et al. 2012). Backstepping control is used for station-keeping control of the USV WAM-V 14 (Sarda et al. 2015) in conditions of fixed positioning. Later, a backstepping adaptive control system is presented by Klinger et al. (2016) for maneuvering the same USV with successful tests in conditions of variable mass and drag. Robust control systems have proven useful in high-speed USVs course tracking. An adaptive sliding mode control of a water-jet (Chen et al. 2017) guaranteed the stability and good course tracking performance through simulations.

For systems with significant nonlinear behavior and large parametric uncertainties, the robust control $\mathcal{H}_\infty$ may not be sufficient to control their dynamics; it is in this field that the linear parameter varying (LPV) control is shown as an appropriate alternative to offer the desired robustness and performance to closed-loop systems. The first approach to the implementation of this type of controller in maritime vehicles is given by the control of an autonomous underwater vehicle named $Aster^x$ (Roche et al. 2009), whereby the mass is the parameter varying. The sub-optimal control problem can be straightforwardly solved using the linear matrix inequalities (LMI). In recent years, some works related to vessel control using LPV controllers were published. In 2015, the adaptive control of the horizontal dynamics of a surface vehicle (Liu et al. 2015) was presented; its results are studied by simulation. More recently, an experimental study of the modeling and identification of a water-jet propulsion USV (Xiong et al. 2014) was proposed with an UKF (unscented Kalman filter) based on active modeling technique to estimate the model error.

2 EDSON-J USV

The EDSON-J vehicle is a Peruvian unmanned surface vehicle under construction by the *University of San Agustín de Arequipa*, whose main mission is to supervise the oceans in the estuary regions. This is a twin-hull vessel class, and its main dimensions are summarized in Table 1.

Figure 1 shows the design of the vehicle, a catamaran structure consisting of two slender bodies connected through a deck. The EDSON-J operates in a cruise speed of 2 m/s and can achieve a maximum speed of 2.7 m/s. The propulsion system of this USV consists of two fixed trolling motors,

Table 1 EDSON-J USV parameters

Parameter	Value
Length	3.00 m
Breadth	1.60 m
Mass	250 kg
Payload	100 kg
Hull breadth	0.30 m
Draft	0.20 m
Inertia moment	201.1 kg/m^2
Location of mass center	0.11 m
Electric motor power (each)	600 W

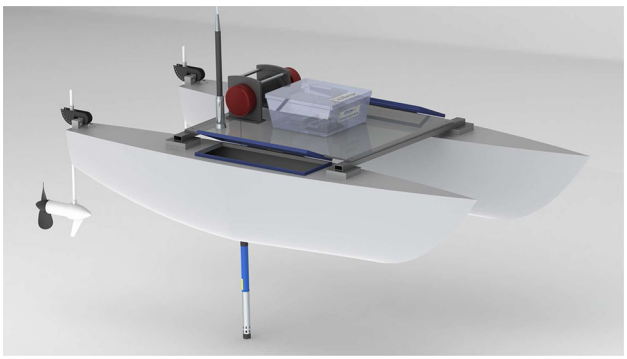

Fig. 1 EDSON-J USV

located at the bow of each hull and working in differential and common modes. The vehicle power supply is given for two 100-Ah AGM batteries that ensure a 5-h autonomy at cruise speed. The navigation of the vehicle is given by a dual GNSS/INS system to ensure the accuracy in the position, velocity and acceleration measures. The communication system is based on RF transceivers, with a range of 60 miles (96.56 km) in the 900 MHz spectrum. The control architecture is distributed between Texas Instrument launchpad microcontrollers and an NVIDIA Jetson TX-2 central computer running on GNU/Linux operative system and powered by a robot operating system (ROS).

2.1 Nonlinear Model

The mathematical model of a vessel can be expressed by considering its horizontal motions and following the SNAME (1950) notation. Figure 2 presents the inertial-frame coordinates of the vehicle composed of surge position x, sway position y and yaw position ψ. The body-frame coordinates of the vehicle are composed of surge velocity u, sway velocity v and yaw velocity r. According to the matrix representation in three degrees of freedom (3-DOF), the position vector relative to inertial-frame is represented by $\boldsymbol{\eta} = \begin{bmatrix} x & y & \psi \end{bmatrix}^{\mathrm{T}}$, the velocity vector relative to the body-frame is represented by

$\boldsymbol{v} = \begin{bmatrix} u & v & r \end{bmatrix}^{\mathrm{T}}$, and the vector of the generalized input forces is represented by $\boldsymbol{\tau}$. The kinematic equations of motion can be expressed in matrix representation as in Fossen (2011):

$$\dot{\boldsymbol{\eta}} = \boldsymbol{J}(\boldsymbol{\eta})\boldsymbol{v}, \tag{1}$$

where $\dot{\boldsymbol{\eta}}$ is the derivative position vector and $\boldsymbol{J}(\boldsymbol{\eta})$ is the coordinate transformation matrix between inertial-frame and body-frame, which is defined as:

$$\boldsymbol{J}(\boldsymbol{\eta}) = \begin{bmatrix} cos(\psi) & -sin(\psi) & 0 \\ sin(\psi) & cos(\psi) & 0 \\ 0 & 0 & 1 \end{bmatrix} \tag{2}$$

The dynamic equations of motion can be expressed as:

$$\boldsymbol{M}\dot{\boldsymbol{v}} + \boldsymbol{C}(\boldsymbol{v})\boldsymbol{v} + \boldsymbol{D}(\boldsymbol{v})\boldsymbol{v} = \boldsymbol{\tau}, \tag{3}$$

where $\boldsymbol{M}$ is the inertia matrix, the $\boldsymbol{C}$ matrix contains Coriolis and rigid body terms, and $\boldsymbol{D}$ is the damping matrix. All these matrices have parameter coefficients that can be obtained through empirical, numerical or computational methods considering the fluid structure interaction. These matrices are as follows:

$$\boldsymbol{M} = \begin{bmatrix} m - X_{\dot{u}} & 0 & 0 \\ 0 & m - Y_{\dot{v}} & mx_g - Y_{\dot{r}} \\ 0 & mx_g - N_{\dot{v}} & I_z - N_{\dot{r}} \end{bmatrix}, \tag{4}$$

$$\boldsymbol{C} = \begin{bmatrix} 0 & -mr & -mx_g r + Y_{\dot{v}} v + Y_{\dot{r}} r \\ mr & 0 & -X_{\dot{u}} u \\ mx_g r - Y_{\dot{v}} v - Y_{\dot{r}} r & X_{\dot{u}} u & 0 \end{bmatrix}, \tag{5}$$

$$\boldsymbol{D} = -\begin{bmatrix} X_u + X_{|u|u}|u| & 0 & 0 \\ 0 & Y_v + Y_{|v|v}|v| & 0 \\ 0 & 0 & N_r + N_{|r|r}|r| \end{bmatrix}, \tag{6}$$

where m is the vehicle mass, x_g is the location of center mass and I_z is the inertia moment around the z axis, $X_{\dot{u}}$, $Y_{\dot{v}}$, $Y_{\dot{r}}$, $N_{\dot{v}}$ and $N_{\dot{r}}$ are the added mass hydrodynamics terms. X_u, Y_v and N_r are the linear drag coefficients. $X_{|u|u}$, $Y_{|v|v}$ and $N_{|r|r}$ are the quadratic drag coefficients.

2.1.1 Hydrodynamic Coefficients

There are many ways to compute the hydrodynamic coefficients of a vessel mainly grouped into analytical, numerical and experimental. For this work, previously successful analytical methods in marine vehicle modeling have been used (Prado 1997; Cutipa-Luque 2012; Prestero 1994; Rentschler 2001). The axial drag terms X_u and X_{uu} are computed by using a graphical method (Harvald 1992); this method relates the geometry of the hull with the resistance expression (Leonessa et al. 2003)

$$R = \frac{1}{2}\rho_f S u^2 C_T, \tag{7}$$

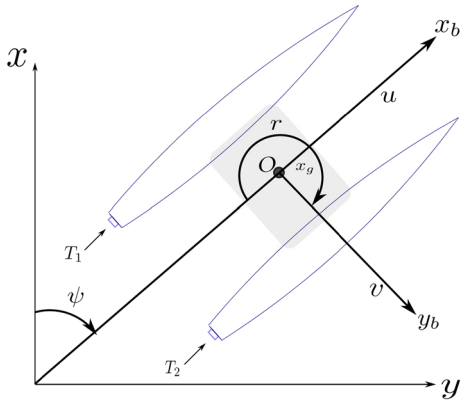

Fig. 2 Coordinates system for the state variables

where ρ_f is the fluid density, S the submerged surface and C_T a nondimensional resistance coefficient. The added mass terms $X_{\dot{u}}, Y_{\dot{v}}, Y_{\dot{r}}, N_{\dot{v}}, N_{\dot{r}}$ and the crossflow drag terms Y_v, N_r, $Y_{|v|v}, N_{|r|r}$ are calculated by using the strip theory (Newman 1979; Prestero 1994) over the added mass coefficient for an ellipse

$$m_a = \frac{\pi}{2}\rho_f T_f^2, \tag{8}$$

where T_f is the vessel draft. The hydrodynamic coefficients shown in Table 2 are computed according to the dimensions and behavior considered for the EDSON-J USV.

2.1.2 Propulsion

The propulsion of the vehicle is given for two MinnKota trolling motors with maximum 18 kg of propulsion each. The propellers can be described by the two following expressions:

$$K_T = \frac{T_p}{\rho_f n^2 D_p^4}, \qquad K_Q = \frac{Q_p}{\rho_f n^2 D_p^5}, \tag{9}$$

where K_T is the nondimensional thrust T_p coefficient, K_Q is the nondimensional torque Q_p coefficient, ρ is the water density, D_p the propeller diameter, and n the rotational velocity. Following the Carlton (2018) approach, the model propeller is obtained using the B series of Wageningen that rearranged the K_T and K_Q coefficients with respect to advance coefficient J and the propeller geometry. These expressions can be approximated through the polynomials:

$$\begin{aligned} K_T &= a_2 J^2 + a_1 J + a_0, \\ K_Q &= b_2 J^2 + b_1 J + b_0, \end{aligned} \tag{10}$$

where $a_0, b_0, a_1, \ldots, b_2$ coefficients are constants as shown in Table 3. Rotational speed n is constrained by the electrical motors features. According to the experimental data in

Table 2 EDSON-J USV parameters

Parameter	Value	Units
$X_{\dot{u}}$	− 2.471	kg
X_u	− 0.291	kg/s
X_{uu}	− 27.626	kg/m
X_{un_c}	− 3.682	kg
X_{rn_d}	1.841	kg m
$X_{n_cn_c}$	1.052	kg m^2
$X_{n_dn_d}$	1.052	kg m^2
$Y_{\dot{v}}$	− 247.065	kg
$Y_{\dot{r}}$	− 370.597	kg m/rad
Y_v	− 123.532	kg/s
Y_{vv}	− 38.928	kg/m
Y_{vn_c}	− 0.359	kg
Y_{rn_c}	− 0.538	kg m
$N_{\dot{r}}$	− 748.310	kg m^2/rad
$N_{\dot{v}}$	− 370.597	kg m
N_r	− 741.195	kg m^2/rad s^2
N_{rr}	− 262.791	kg m^2/rad^2
N_{un_d}	2.762	kg m
N_{rn_c}	− 2.855	kg m^2
$N_{n_cn_d}$	− 1.578	kg m^2
N_{vn_c}	− 0.538	kg m

Table 3 Propeller coefficients

K_T	K_Q
$a_0 = 0.1884$	$b_0 = 0.0113$
$a_1 = -0.1507$	$b_1 = -0.0325$
$a_2 = -0.1132$	$b_2 = -0.0102$

Prado (1997), a maximum rotational speed $n_{\max} = 22$ rps is considered for a maximum vehicle speed $u_{\max} = 2.7$ m/s. Both propeller rotational velocities n_1 and n_2 are replaced by their values in common mode (n_c) and differential mode (n_d), such as:

$$n_c = \frac{n_1 + n_2}{2}, \qquad n_d = \frac{n_1 - n_2}{2}. \tag{11}$$

2.2 LPV Model

This section presents the EDSON-J LPV model considering a twin-hull based vessel, designed to carry out missions of maritime supervision, transporting instruments and specialized multiparameter sondes to automatically measure water quality. Therefore, the vehicle is able to carry out variable mass payload. From the nonlinear model described in (1) and (3), the LPV system is represented in state space equations with ρ as a depending parameter:

$$G(\rho): \begin{cases} \dot{\mathtt{x}} = A(\rho)\mathtt{x} + B(\rho)\mathtt{u} \\ \mathtt{y} = C(\rho)\mathtt{x} + D(\rho)\mathtt{u} \end{cases}, \tag{12}$$

where $\mathtt{x} = [u\ v\ r]^{\mathrm{T}}$ is the state vector, $\mathtt{u} = [n_c\ n_d]^{\mathrm{T}}$ is the control input vector, $\mathtt{y} = [u\ r]^{\mathrm{T}}$ is the measured output vector and ρ is the set of parameters varying, being $\underline{\rho}$ the minimum value and $\overline{\rho}$ the maximum. In this work, due to possible payloads changes, vehicle mass m is the chosen varying parameter to be studied. Then, it considers ρ with $(\underline{\rho}, \overline{\rho}) = [250 : 350]$ kg. More parameters, such as the drag forces or the water density, can be chosen, but they could compromise the controller complexity. The values for the $A(\rho)$, $B(\rho)$, $C(\rho)$ and $D(\rho)$ matrix are obtained by Jacobian linearization over the cruise speed operation point $u_0 = 2.0$ m/s, $n_0 = 14$ rps and ρ. For more details about the state space matrix representation, see Pérez and Blanke (2002).

3 LPV/$\mathcal{H}_\infty$ Control

3.1 $\mathcal{H}_\infty$ Control for LPV Systems

The generalized plant for LTI/$\mathcal{H}_\infty$ robust control synthesis approach is well established in the literature (Skogestad and Postlethwaite 2007). Then, the LPV generalized plant matrix form $\boldsymbol{\Sigma(\rho)}$ can be expressed as:

$$\boldsymbol{\Sigma}(\rho): \begin{bmatrix} \dot{\mathtt{x}} \\ \mathtt{z} \\ \mathtt{y} \end{bmatrix} = \left[\begin{array}{c|cc} A(\rho) & B_1(\rho) & B_2(\rho) \\ \hline C_1(\rho) & D_{11}(\rho) & D_{12}(\rho) \\ C_2(\rho) & D_{21}(\rho) & D_{22}(\rho) \end{array}\right] = \begin{bmatrix} \mathtt{x} \\ \mathtt{w} \\ \mathtt{u} \end{bmatrix}, \tag{13}$$

where $\mathtt{w} \in \mathbb{R}^q$ is the exogenous input vector, $\mathtt{y} \in \mathbb{R}^p$ is the measured output vector, $\mathtt{u} \in \mathbb{R}^m$ is the control input control vector, and $\mathtt{z} \in \mathbb{R}^r$ is the exogenous output vector, or also named performance output vector.

The LPV controller $\boldsymbol{K}(\rho)$ can be described as:

$$\boldsymbol{K}(\rho): \begin{bmatrix} \dot{\mathtt{x}}_c \\ \mathtt{u} \end{bmatrix} = \begin{bmatrix} A_c(\rho) & B_c(\rho) \\ C_c(\rho) & D_c(\rho) \end{bmatrix} = \begin{bmatrix} \mathtt{x}_c \\ \mathtt{y} \end{bmatrix}, \tag{14}$$

where $\mathtt{x}_c \in \mathbb{R}^n$ is the state vector of the controller. $A_c(\rho)$, $B_c(\rho)$, $C_c(\rho)$, $D_c(\rho)$, are continuous bounded matrix functions. The closed-loop system is found using linear fractional transformation (LFT) through relation $\boldsymbol{\Sigma_{CL}}(\rho) = LFT(\boldsymbol{\Sigma}(\rho), \boldsymbol{K}(\rho))$ and expressed in state space form as:

$$\boldsymbol{\Sigma_{CL}}(\rho): \begin{bmatrix} \dot{\xi} \\ \mathtt{z} \end{bmatrix} = \begin{bmatrix} \boldsymbol{\mathcal{A}}(\rho) & \boldsymbol{\mathcal{B}}(\rho) \\ \boldsymbol{\mathcal{C}}(\rho) & \boldsymbol{\mathcal{D}}(\rho) \end{bmatrix} \begin{bmatrix} \xi \\ \mathtt{w} \end{bmatrix}, \tag{15}$$

where

$$\begin{cases} \mathcal{A} = \begin{pmatrix} A(\rho) + B_2(\rho)D_c(\rho)C_2(\rho) & B_2(\rho)C_c(\rho) \\ B_c(\rho)C_2(\rho) & A_c(\rho) \end{pmatrix} \\ \mathcal{B} = \begin{pmatrix} B_1(\rho) + B_2(\rho)D_c(\rho)D_{21}(\rho) \\ B_c(\rho)D_{21}(\rho) \end{pmatrix} \\ \mathcal{C} = \begin{pmatrix} C_1(\rho) + D_{12}(\rho)D_c(\rho)C_2(\rho) & D_{12}(\rho)C_c(\rho) \end{pmatrix} \\ \mathcal{D} = \begin{pmatrix} D_{11}(\rho) + D_{12}(\rho)D_c(\rho)D_{21}(\rho) \end{pmatrix} \end{cases}, \quad (16)$$

with $\xi = [\mathrm{x}^{\mathrm{T}} \ \ \mathrm{x}_c^{\mathrm{T}}]^{\mathrm{T}} \in \mathbb{R}^{2n}$, The control objective is to find controller $\boldsymbol{K}(\rho)$ that minimizes the induced $\mathcal{L}_2$ norm of the closed-loop LPV system (15):

$$||\boldsymbol{\Sigma}_{\mathcal{CL}}(\boldsymbol{\rho})||_{2\to 2} = \sup_{\substack{\rho\in\mathcal{P} \\ \bar{\nu}\le\dot{\rho}\le\underline{\nu}}} \sup_{\substack{\mathrm{w}\in\mathcal{L}_2 \\ ||\mathrm{w}||_2\neq 0}} \frac{||\mathrm{z}||_2}{||\mathrm{w}||_2} \quad (17)$$

3.2 Solution to the LPV Problem Based on LMIs

This section gives the theory for solving the LPV problem. This theorem describes the LPV problem in terms of the induced $\mathcal{L}_2$ norm (Wu 1995; Wu et al. 1996):

Theorem 1 *Given a compact set $\mathcal{P} \in \mathbb{R}^s$, $\mathcal{S}^{nxn}$ a set of symmetric matrices in $\mathbb{R}^{nxn}$, the rate bounds $(\bar{\nu}, \underline{\nu})$, the performance level γ and the LPV system $\boldsymbol{\Sigma}(\boldsymbol{\rho})$, the parameter-dependent performance problem has a solution if there are continuously differentiable matrix functions $X : \mathbb{R}^s \to \mathcal{S}^{nxn}$, and $Y : \mathbb{R}^s \to \mathcal{S}^{nxn}$, such that for all $\rho \in \mathcal{P}$, $X(\rho) > 0$, $Y(\rho) > 0$ and*

$$\begin{bmatrix} M(\rho) & C_{11}(\rho)X(\rho) & \gamma^{-1}B_1(\rho) \\ C_{11}(\rho)X(\rho) & -I_r & 0 \\ \gamma^{-1}B_1^{\mathrm{T}}(\rho) & 0 & -I_q \end{bmatrix} < 0, \quad (18)$$

where

$$M(\rho) = \hat{A}(\rho)X(\rho) + X(\rho)\hat{A}^{\mathrm{T}}(\rho) - \sum_{i=1}^{s} \pm \left(\nu_i \frac{\delta X(\rho)}{\delta \rho_i}\right) - B_2(\rho)B_2^{\mathrm{T}}(\rho)$$

$$\begin{bmatrix} N(\rho) & Y(\rho)B_{11}(\rho) & \gamma^{-1}C_1^{\mathrm{T}}(\rho) \\ B_{11}^{\mathrm{T}}(\rho)Y(\rho) & -I_q & 0 \\ \gamma^{-1}C_1(\rho) & 0 & -I_r \end{bmatrix} < 0, \quad (19)$$

where

$$N(\rho) = \tilde{A}^{\mathrm{T}}(\rho)Y(\rho) + Y(\rho)\tilde{A}^{\mathrm{T}}(\rho) + \sum_{i=1}^{s} \pm \left(\nu_i \frac{\delta Y(\rho)}{\delta \rho_i}\right) - C_2^{\mathrm{T}}(\rho)C_2(\rho)$$

$$\begin{bmatrix} X(\rho) & \gamma^{-1}I_n \\ \gamma^{-1}I_n & Y(\rho) \end{bmatrix} \geq 0, \quad (20)$$

$\hat{A}(\rho) = A(\rho) - B_2(\rho)C_{12}(\rho)$, $\tilde{A}(\rho) = A(\rho) - B_{12}(\rho)C_2(\rho)$. *If the conditions are satisfied, there is a controller $\boldsymbol{K}(\rho)$ that solves the problem.*

The infinite-dimensional space function problem can be parametrized through a finite set of continuously differentiable functions $\{f_i : \mathbb{R}^s \to \mathbb{R}\}_{i=1}^{N_x}$,$\{g_i : \mathbb{R}^s \to \mathbb{R}\}_{j=1}^{N_y}$ for the matrices $X, Y : \mathbb{R}^s \to \mathcal{S}^{nxn}$, such that:

$$X(\rho) = \sum_{i=1}^{N_x} f_i(\rho)X_i, \quad Y(\rho) = \sum_{j=1}^{N_y} g_i(\rho)Y_j \quad (21)$$

The solution of this convex optimization problem requires gridding set ρ at L points $\{\rho_k\}_{k=1}^{L}$. The density of these grid points is defined by the following lemma:

Lemma 1 *Assume a continuously differentiable state-space data and twice continuously differentiable functions f_i, g_i. Let*

$$\begin{aligned} h_{\min} := \delta_{\min} \Bigg\{ \Bigg[& 2T \sum_{i=1}^{N} \max_{\rho\in\mathcal{P}} \left\| \frac{d(g_i\hat{A}^{\mathrm{T}})}{d\rho} \right\|_F \\ & + \nu T \sum_{i=1}^{N} \max_{\rho\in\mathcal{P}} \left| \frac{d^2 g_i}{d\rho^2} \right| + \gamma \max_{\rho\in\mathcal{P}} \left\| \frac{d(B_2B_2^{\mathrm{T}})}{d\rho} \right\|_F \\ & + 2T \sum_{i=1}^{N} \max_{\rho\in\mathcal{P}} \left\| \frac{d(g_iC_{11}^{\mathrm{T}})}{d\rho} \right\|_F + 2\max_{\rho\in\mathcal{P}} \left| \frac{d^2B_1}{d\rho} \right|_F \Bigg]^{-1}, \\ & \Bigg[2T \sum_{i=1}^{N} \max_{\rho\in\mathcal{P}} \left\| \frac{d(f_i\hat{A}^{\mathrm{T}})}{d\rho} \right\|_F \\ & + \nu T \sum_{i=1}^{N} \max_{\rho\in\mathcal{P}} \left| \frac{d^2 f_i}{d\rho^2} \right| + \gamma \max_{\rho\in\mathcal{P}} \left\| \frac{d(C_2C_2^{\mathrm{T}})}{d\rho} \right\|_F \\ & + 2T \sum_{i=1}^{N} \max_{\rho\in\mathcal{P}} \left\| \frac{d(f_iB_{11}^{\mathrm{T}})}{d\rho} \right\|_F + 2\max_{\rho\in\mathcal{P}} \left| \frac{d^2C_1}{d\rho} \right|_F \Bigg]^{-1}, \\ & \Bigg[T \sum_{i=1}^{N} \max_{\rho\in\mathcal{P}} \left| \frac{d(f_i)}{d\rho} \right| + T \sum_{i=1}^{N} \max_{\rho\in\mathcal{P}} \left| \frac{d(g_i)}{d\rho} \right| \Bigg]^{-1} \Bigg\} \end{aligned} \quad (22)$$

where $T > 0$ is a larger number, $\delta > 0$ is a smaller number and F is the state-feedback gain. A $|\rho_k - \rho_{k+1}| \leq h_{\min}$ for all $k = 1, \ldots, L-1$ guarantee that the grid density solves the LMIs problem.

Since $\rho \in \mathbb{R}^s$ a total of $L^s(2^{s+1}+1)$ LMIs in terms of X_i and Y_i must be solved.

4 Methodology

The robustness and performance of the control system is formulated in the $\mathcal{H}_\infty$ framework. In this section, the per-

formance specifications and control structure of the LPV controller proposed for the EDSON-J are presented.

4.1 Weighting Functions

In order to set some specifications of robustness and performance in closed loop, we must choose suitable weighting functions (Zhou and Doyle 1998).

The sensitivity function $\boldsymbol{S} = (I + G\boldsymbol{K})^{-1}$, related to good tracking and good disturbance rejection, is weighted by $W_S = \text{diag}[W_{S_u}, W_{S_r}]$ in surge velocity u and in yaw rate r directions, respectively:

$$W_{S_u} = \frac{s/M_u + \omega_u}{s + \omega_u \epsilon_u}, \qquad W_{S_r} = \frac{s/M_r + \omega_r}{s + \omega_r \epsilon_r}, \tag{23}$$

where $M_u = M_r = 2$ are the D.C. gains of the functions which control the disturbance rejection, $\omega_u = 2$ and $\omega_r = 0.5$ are the bandwidth of the closed-loop response and $\epsilon_u = \epsilon_r = 0.01$ are small and finite values to avoid numerical singularities in the computation.

The function $W_C = \text{diag}[W_{C_{n_c}}, W_{C_{n_d}}]$ weights the controller sensitivity function $\boldsymbol{KS}$ that restricts the control input according to the actuators limits

$$W_{C_{n_c}} = \frac{s + \omega_{n_c}/M_{n_c}}{\epsilon_{n_c} s + \omega_{n_c}}, \qquad W_{C_{n_d}} = \frac{s + \omega_{n_d}/M_{n_d}}{\epsilon_{n_d} s + \omega_{n_d}}, \tag{24}$$

where $M_{n_c} = 500$ and $M_{n_d} = 200$ are the magnitude of C, $\omega_{n_c} = 20{,}000$ and $\omega_{n_d} = 2000$ are the bandwidth of the controller and $\epsilon_u = \epsilon_r = 0.001$ are small values that allow implementation. Both input and output disturbance in the generalized plant are not weighted and then $W_{d_i} = W_{d_o} = I_2$.

4.2 TDOF Controller

A centralized controller with two-degree-of-freedom (TDOF) structure is chosen with the form $\boldsymbol{K} = [\boldsymbol{K}_r \ \boldsymbol{K}_y]^{\mathrm{T}}$. This structure was proposed initially in Lundstrom et al. (1999) with the ability to increase performance without compromising the robustness in stability. Figure 3 presents the respective two-port diagram with generalized plant $\boldsymbol{\Sigma}(\rho)$ and controller $\boldsymbol{K}(\rho)$. The generalized plant includes the four weighting functions represented by W_*. The $\mathtt{w} = \left[\mathtt{d}_i \ \mathtt{d}_o \ \mathtt{r}\right]^{\mathrm{T}}$ represents the exogenous inputs, where $\mathtt{r} = \left[u_r \ r_r\right]^{\mathrm{T}}$ is the reference signal for the surge velocity u m/s and the yaw rate r rad/s, respectively. The output performance is given by $\mathtt{z} = [\mathtt{e} \ \mathtt{u}]^{\mathrm{T}}$, where $\mathtt{e} = [u_e \ r_e]^{\mathrm{T}}$ is the error value between the measured output $\mathtt{y} = [u_y \ r_y]^{\mathrm{T}}$ and the reference signal in surge u and yaw r. The control input is given by $\mathtt{u} = [n_c \ n_d]^{\mathrm{T}}$.

The closed-loop transfer function from exogenous input to performance output of the EDSON-J USV can be expressed

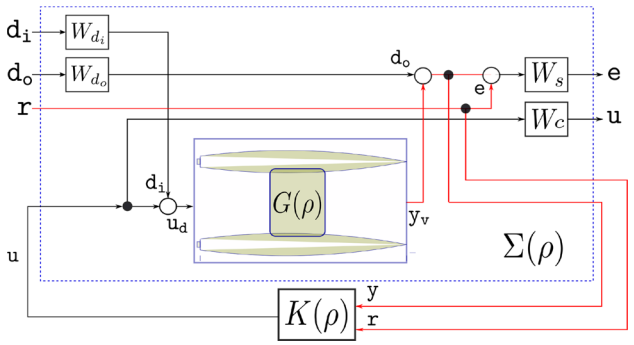

Fig. 3 Closed-loop generalized plant and TDOF controller structure

Table 4 Basis functions and sub-optimal gamma value

$f_i(\rho) = g_i(\rho)$	γ
1	1.0650
$1, \rho$	1.0637
$1, \rho, \rho^2$	1.0637
$1, \rho, \rho^2, \rho^3$	1.0635
$1, \rho, \rho^2, \rho^3, \rho^4$	1.0636
$1, \rho, \rho^2, \rho^3, \rho^4, \rho^5$	0.9180

with respect to the TDOF controller structure as:

$$\begin{bmatrix} \mathtt{e} \\ \mathtt{u} \end{bmatrix} = \begin{bmatrix} \boldsymbol{SG} & \boldsymbol{S} & I - \boldsymbol{SGK}_r \\ I - \boldsymbol{S}\,\boldsymbol{K}_y\boldsymbol{S} & & \boldsymbol{SK}_r \end{bmatrix} \begin{bmatrix} \mathtt{d}_i \\ \mathtt{d}_o \\ \mathtt{r} \end{bmatrix} \tag{25}$$

4.3 LPV Grid Model

For representing the varying parameter dependence, a grid-based model is used; the LPV system is built from a collection of linearizations on the parameters varying gridded domain $\rho \in \mathcal{P}$, the set of LTI systems in the grid is defined for each ρ_k value, where k is the kth grid-point. For this approach, six uniformly spaced points of the mass payload m_p are chosen to grid the interval $\mathcal{P} = [250 \text{ kg}, 350 \text{ kg}]$. To find the basis functions $f_i(\rho)$ and $g_i(\rho)$, different functions with the form ρ^n with $n = 0, 1, 2, \ldots, n$ have been evaluated. The results as a function of performance level are shown in Table 4.

Since an optimal controller must have a performance level $\gamma < 1$, the basis functions are chosen as follows $\{f_i(\rho)\}_{k=1}^6 = \{g_i(\rho)\}_{k=1}^6 = \{1, \rho, \rho^2, \rho^3, \rho^4, \rho^5\}$, other basis functions can be implemented but compromise the optimization time. A good criterion for choosing basis functions is the simplicity. Hence, the parameter-dependent $X(\rho)$ and $Y(\rho)$ are in the form of $X(\rho) = \sum_{i=1}^6 f_i(\rho) X_i$, $Y(\rho) = \sum_{i=1}^6 f_i(\rho) Y_i$.

5 Analysis and Results

This section presents different scenarios to analyze the results and to validate the proposed control strategy, in both frequency domain and time domain. These numerical simulations guarantee the achievement of control goals and allow evaluating the performance of the EDSON-J control system in typical missions, such as supervising estuary regions at sea with different payload instrumentation.

5.1 Frequency-Domain Analysis

The frequency-domain analysis over the augmented plant of the EDSON-J LPV model is shown in Fig. 3. It serves to evaluate the performance and robustness in all set of grid points $\rho \in \mathcal{P} = [250; 270; 290; 310; 330; 350]$ of the controlled system through sensitivity $\boldsymbol{S}$ and controller sensitivity $\boldsymbol{KS}$ functions, and in comparison with a standard LTI/$\mathcal{H}_\infty$ controller, as shown below.

5.1.1 Sensitivity

Figure 4a presents the surge u sensitivity function $\boldsymbol{S}_u$ for the LPV/$\mathcal{H}_\infty$ approach. The $\boldsymbol{S}_u$ LPV/$\mathcal{H}_\infty$ achieves a crossover frequency of 4.3 rad/s and is considered good tracking and rejection to environmental disturbances, such as waves, currents and wind. The main improvement of the LPV/$\mathcal{H}_\infty$ sensitivity function is that the signal never overshoots the design condition $1/W_{S_u}$ unlike the LTI/$\mathcal{H}_\infty$ controller, which crosses the weighting function close to the crossover region between frequencies 0.7 and 2 rad/s.

Figure 4b presents yaw r sensitivity function $\boldsymbol{S}_r$, signal $\boldsymbol{S}_r$ LTI/$\mathcal{H}_\infty$ overshoots the design condition in 5 dB in the low frequencies until 0.1 rad/s, compromising the tracking response and disturbance rejection; signal $\boldsymbol{S}_r$ LPV/$\mathcal{H}_\infty$ with crossover frequency 1.4 rad/s shows a performance improvement because it does not cross weighting function $1/W_{S_r}$.

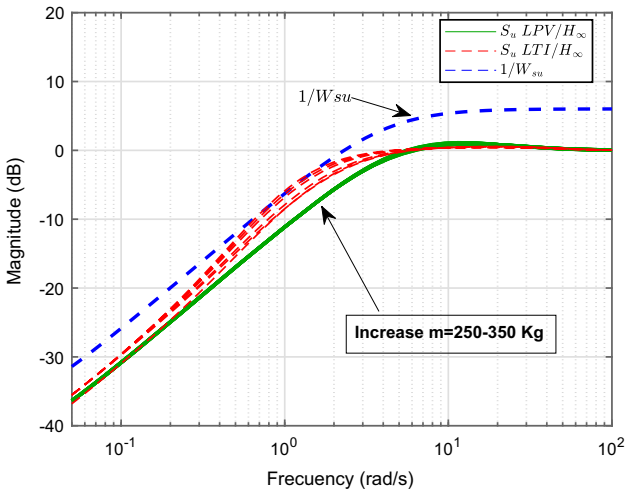

(a) Surge u sensitivity.

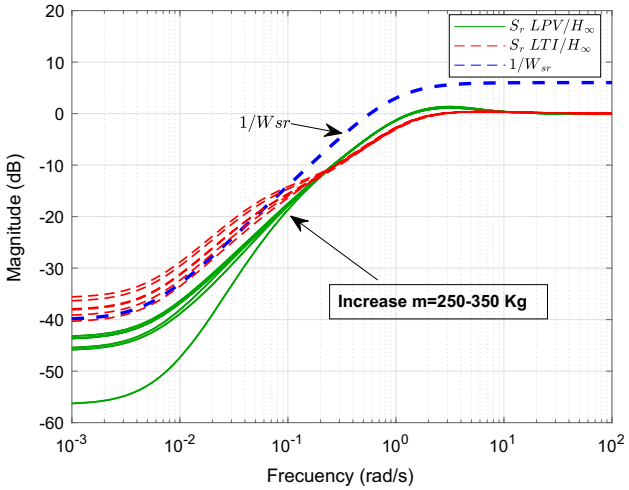

(b) Yaw r sensitivity.

Fig. 4 Sensitivity S performance

5.1.2 Controller Sensitivity

Figure 5a presents the controller sensitivity function $\boldsymbol{KS}_{n_c}$ with a similar behavior in the LPV/$\mathcal{H}_\infty$ and the LTI/$\mathcal{H}_\infty$ approach achieving the control objectives defined by $1/W_{C_{n_d}}$ with a crossover frequency of 400 rad/s.

Figure 5b shows the control sensitivity in differential mode $\boldsymbol{KS}_{n_d}$. Here, the LPV/$\mathcal{H}_\infty$ solution shows a compactness set of signals as a function of parameter varying ρ with a crossover frequency of 58 rad/s in comparison with KS_{nd} LTI/$\mathcal{H}_\infty$ signal, which overshoots the design condition in the frequency of 40 rad/s, causing saturation in the actuators and amplifying measurement noises.

5.2 Time-Domain Analysis

The time-domain responses with the full 3-DOF EDSON-J nonlinear model are simulated using the Simulink according to the scheme presented in Fig. 6. Velocity vector $\boldsymbol{\nu} = [u\ v\ r]$ represents the linear and angular velocities of the USV, $\boldsymbol{\eta} = [x\ y\ \psi]$ represents the inertial frame positions, and $\boldsymbol{\tau}$ is the vector of generalized input forces. A simple guidance LOS system (Caccia et al. 2005) was implemented to evaluate usual maritime missions. Three scenarios have been contemplated to evaluate the performance of the controlled nonlinear EDSON-J model. The proofs have been designed to verify different aspects of the vehicle behavior.

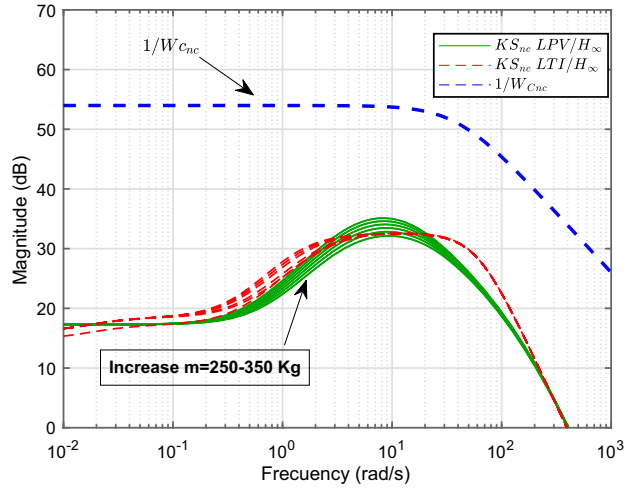

(a) Common mode n_c control sensitivity.

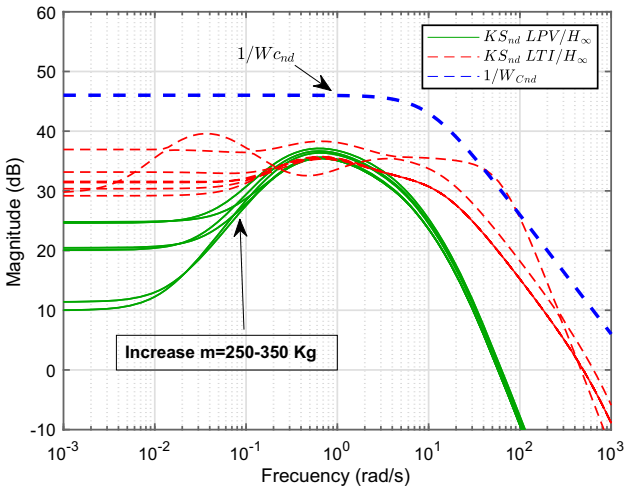

(b) Differential mode n_d control sensitivity.

Fig. 5 Sensitivity control C performance

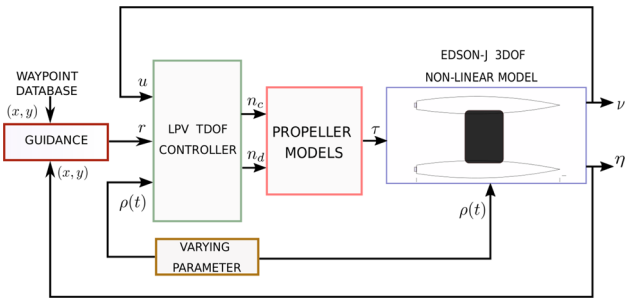

Fig. 6 Diagram of EDSON-J nonlinear simulator

Scenario 1: Stability and Time Response

This test validates the controller in function of stability and compares the time responses of the controlled outputs u, r between the proposed LPV/$\mathcal{H}_\infty$ and a LTI/$\mathcal{H}_\infty$ controller. The test measures velocity surge u m/s and yaw rate r rad/s

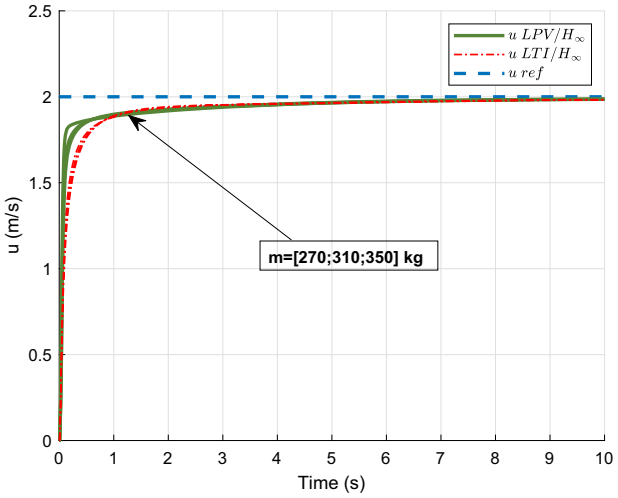

(a) Surge u time response.

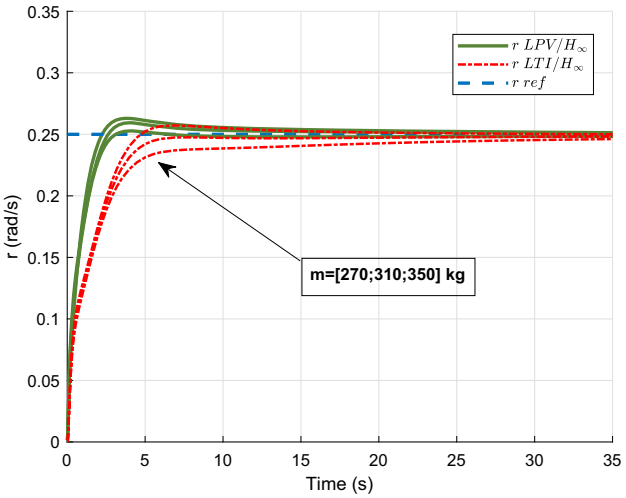

(b) Yaw r time response.

Fig. 7 Time-domain response of the controlled outputs

responses in three operations points $\rho = [270; 310; 350]$ kg representing variations in mass m due to different payloads. Constant reference signals $u = 2.0$ m/s and $r = 0.25$ rad/s are considered. Figure 7 presents the time-domain responses with constant input reference signals. Surge velocity u in three operation points ρ is shown in 7(a). It is possible to note a 0.5 s fast rise time of the LPV/$\mathcal{H}_\infty$ controlled output with respect to standard LTI/$\mathcal{H}_\infty$ with 0.9 s. This is directly related to the frequency behavior in Fig. 4. The responses are not influenced by the increased vehicle payload with a settling time of 4.6 s without overshoots in either controller.

Figure 7b presents an improvement in the worst payload case $m = 350$ kg of 12.46 s in yaw rate r settling time in comparison with the LTI/$\mathcal{H}_\infty$ controller of 23.66 s, the LPV/$\mathcal{H}_\infty$ response is less influenced by the payload changes

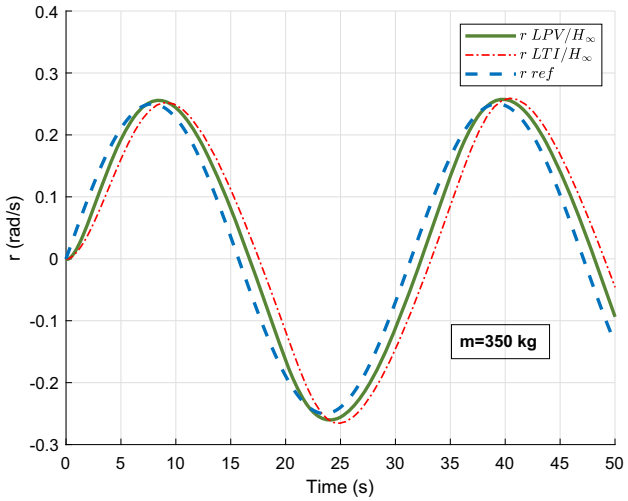

(a) Yaw rate tracking of reference signal.

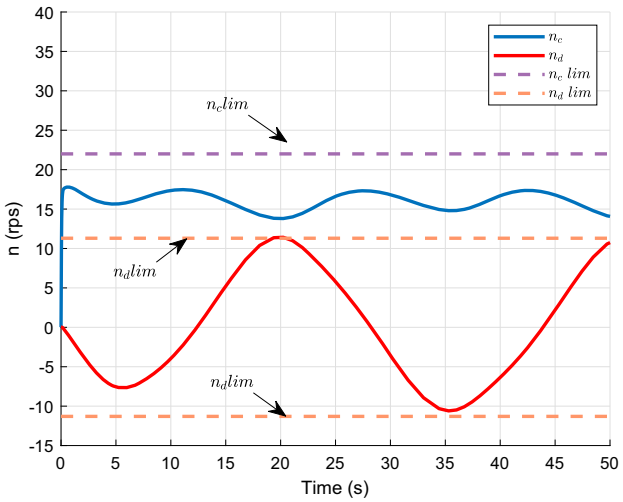

(b) Control effort and actuator limits.

Fig. 8 Control effort for the tracking reference test

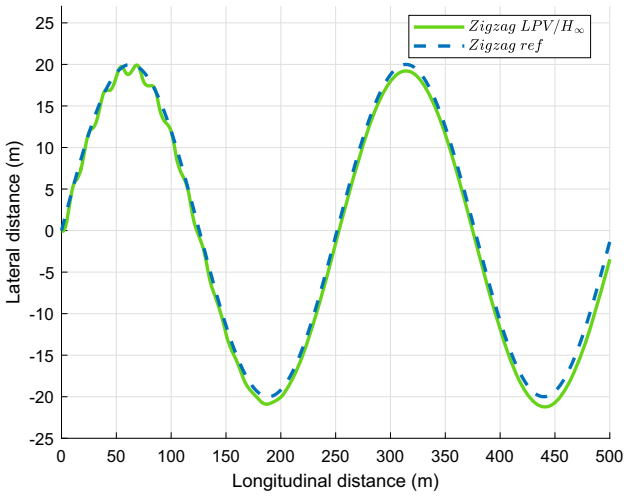

(a) Zigzag trajectory.

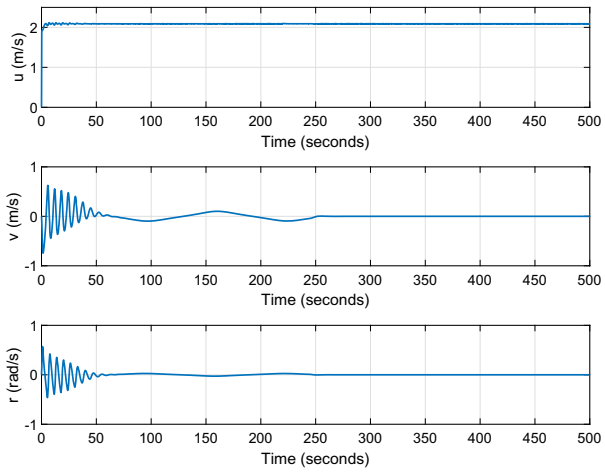

(b) Nonlinear parameters in zigzag maneuver.

Fig. 9 Zigzag maneuver

and compactness. A better rise time 3.14 s and settling time is obtained with a little overshoot of 5.2 %.

Scenario 2: Tracking and Control Effort

For the second test, it has been considered a time-varying reference signal for input yaw rate r, represented by a sine function with a peak amplitude of 0.25 rad/s. The good tracking of yaw r is essential for the horizontal maneuvering performed. For this simulation, the worst case $m = 350$ kg is presented and velocity surge u is kept to be a constant value of $u = 2$ m/s. Figure 8a shows a good tracking performance of varying reference signal yaw r rad/s. The LPV/$\mathcal{H}_\infty$ approach has a lower tracking error that the LTI/$\mathcal{H}_\infty$ controller.

Figure 8b presents the control effort and the actuator limits. With the surge velocity set at 2 m/s, the yaw rate tracks the sinusoidal reference between -0.3 and 0.3 rad/s, achieving a maximum control effort of $n_c = 18$ rps and $n_d = 11$ rps, lower than the limits and constraint imposed by the class propeller used ($n_c = 22$ and $n_d = 11$ rps, see section 2 for details).

Scenario 3: Usual Maneuvers

With guaranteed stability, tracking performance and control effort allowed, the next step is performing maneuvering tests, bridging the gap between purely theoretical analysis and real-world applications. For the third test, a simple guidance system has been implemented that allows performing classic maneuvers. Two maneuvers are studied: zigzag in Fig. 9 and circular in Fig. 10; both simulations consider a mass $m = 300$ kg.

Figure 9a presents a path-following type zigzag, represented by a sinusoidal trajectory wave with 40 m of amplitude

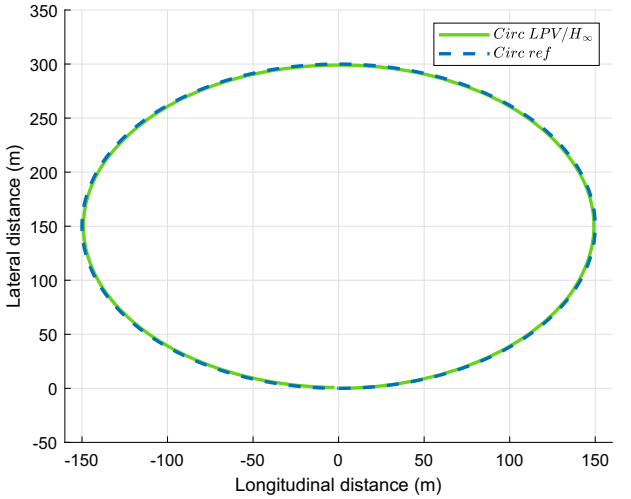

(a) Circular trajectory.

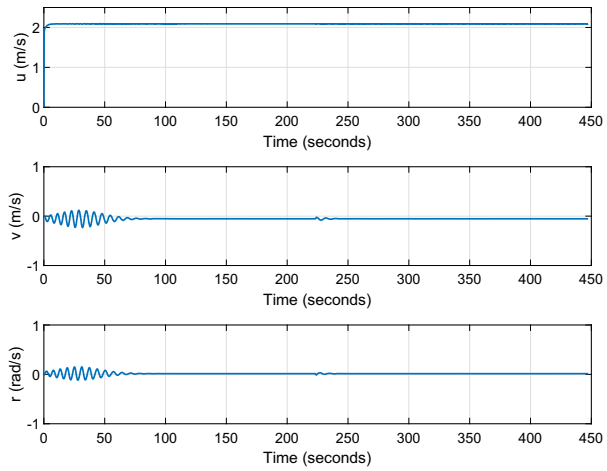

(b) Nonlinear parameters in Circular maneuver.

Fig. 10 Circular maneuver

and a period of 250 m; the trajectory of the USV has a maximum tracking error of less than 1 m. Figure 9b presents velocities $\boldsymbol{v} = [u\ v\ r]$ during this path-following trajectory; surge velocity u quickly achieves the condition proposed of 2 m/s without steady-state errors, v and r present oscillatory transitions during the first 50 s until achieving the steady state.

Figure 10a presents the vehicle following a circular path; the reference trajectory is a circle with a radio of 150 m. The trajectory of the EDSON-J presents no considerable errors with respect to the circular desired trajectory. Figure 10b presents the nonlinear velocities during the circular test; velocity surge u has a steady-state response of 2 m/s, sway velocity v and yaw rate r present oscillatory in transient responses, but these are lower compared with the last zigzag path-following trajectory.

6 Conclusions

The synthesis of a robust LPV controller using a grid-based approach for the LPV/$\mathcal{H}_\infty$ control of EDSON-J USV with mass variation due to different payload instrumentation is successfully validated. A centralized two-degree-of-freedom (TDOF) controller structure achieves the frequency-domain responses goals ensuring the robustness, stability and tracking performance for all the set of varying parameters ρ of the USV. Using the nonlinear EDSON-J simulator, time-domain responses and guidance tests during circular and zigzag path-following trajectories determine the feasibility of the proposed robust control approach, significantly improving its performances compared with the LTI/$\mathcal{H}_\infty$, despite the conditions of mass variation and actuator saturation limits. The choice of basis functions and weighting functions has proven to be essential to achieve the design objectives. Depending on these goals, other approaches for getting these expressions can be considered. In further works, other varying parameters can be considered, such as drag forces or fluid conditions. These numerical results allow continuing the implementation phase and subsequent experimental tests with the EDSON-J vehicle. A complete EDSON-J USV model with 6-DOF and environmental models is under consideration.

Acknowledgements The authors thank the *Universidad Nacional de San Agustín de Arequipa* for supporting this research since 2019 under Grant No. IBAIB-08-2018-UNSA. The authors thank Prof. Dr. Antonio Pascoal for sharing essential information for the development of this work.

References

Alves, J., Oliveira, P., Oliveira, R., Pascoal, A., Rufino, M., Sebastiao, L., & Silvestre, C. (2006). Vehicle and mission control of the delfim autonomous surface craft. In: *2006 14th mediterranean conference on control and automation* (pp 1–6). IEEE.

Caccia, M., Bibuli, M., Bono, R., Bruzzone, G., Bruzzone, G., & Spirandelli, E. (2007). Unmanned surface vehicle for coastal and protected waters applications: The charlie project. *Marine Technology Society Journal*, *41*(2), 62–71.

Caccia, M., Bono, R., Bruzzone, G., Spirandelli, E., Veruggio, G., Stortini, A., et al. (2005). Sampling sea surfaces with sesamo: An autonomous craft for the study of sea–air interactions. *IEEE Robotics Automation Magazine*, *12*(3), 95–105.

Carlton, J. (2018). *Marine propellers and propulsion*. Oxford: Butterworth-Heinemann.

Chen, X., Liu, Z., Hu, H., Wang, L., & Dong, J. (2017). Backstepping adaptive sliding mode control for the usv course tracking system. In: *2017 9th international conference on advanced infocomm technology (ICAIT)* (pp 265–269). IEEE.

Cutipa-Luque, J. C. (2012). Identificaão e controle de um veículo submersível autônomo sub-atuado. Ph.D. thesis, Escola Politécnica da Universidade de São Paulo, São Paulo

Cutipa-Luque, J. C., Donha, D. C., Dantas, J. L. D., de Oliveira, L. M., & de Barros, E. A. (2012). Robust control of an underactuated AUV. *IFAC Proceedings Volumes*, *45*(27), 138–143.

Fossen, T. I. (2011). *Handbook of marine craft hydrodynamics and motion control*. New York: Wiley.

Harvald, S. A. (1992). Resistance and propulsion of ships

Klinger, W. B., Bertaska, I. R., von Ellenrieder, K. D., & Dhanak, M. R. (2016). Control of an unmanned surface vehicle with uncertain displacement and drag. *IEEE Journal of Oceanic Engineering*, *42*(2), 458–476.

Leonessa, A., Mandello, J., Morel, Y., Vidal, M. (2003). Design of a small, multi-purpose, autonomous surface vessel. In: *Oceans 2003. Celebrating the past... teaming toward the future (IEEE Cat. No. 03CH37492)* (Vol. 1, pp. 544–550). IEEE.

Liu, Z., Yuan, C., & Zhang, Y. (2015). Linear parameter varying adaptive control of an unmanned surface vehicle. *IFAC-Papers OnLine*, *48*(16), 140–145.

Lundstrom, P., Skogestad, S., & Doyle, J. C. (1999). Two-degree-of-freedom controller design for an ill-conditioned distillation process using/spl mu/-synthesis. *IEEE Transactions on Control Systems Technology*, *7*(1), 12–21.

Luque, J., & Donha, D. (2008). Two dof robust controller for a six dof underwater autonomous vehicle. In *ABCM symposium series in mechatronics* (Vol. 3, pp. 217–224).

Manley, J. E. (2008). Unmanned surface vehicles, 15 years of development. In: *OCEANS 2008* (pp. 1–4). IEEE

Manley, J. E., Marsh, A., Cornforth, W., & Wiseman, C. (2000). Evolution of the autonomous surface craft autocat. In: *OCEANS 2000 MTS/IEEE conference and exhibition. Conference proceedings (Cat. No. 00CH37158)* (Vol 1, pp. 403–408). IEEE.

Martins, A., Ferreira, H., Almeida, C., Silva, H., Almeida, J. M., & Silva, E. (2007). Roaz and Roaz ii autonomous surface vehicle design and implementation. In: *International lifesaving congress 2007*

Newman, J. N. (1979). *Theoretical methods in ship maneuvering*. Technical reports. Massachusetts Institute of technology.

Pérez, T., & Blanke, M. (2002). Mathematical ship modeling for control applications.

Prado, M. G. (1997). Modelizacão e controlo de um veículo oceanográfico autónomo. Master's thesis, Universidade Técnica de Lisboa

Prestero, T. (1994). Verification of a six-degree of freedom simulation model for the remus auv. Master's thesis, Massachusetts Institute of Technology.

Rentschler, M. E. (2001). Dynamic simulation modelling and control of the odyssey iii autonomous underwater vehicle. Master's thesis, Massachusetts Institute of Technology.

Roche, E., Sename, O., & Simon, D. (2009). Lpv/h control of an autonomous underwater vehicle (auv). In: *2009 European control conference (ECC),* (pp 3160–3165). IEEE.

Sarda, E. I., Bertaska, I. R., Qu, A., & von Ellenrieder, K. D. (2015). Development of a usv station-keeping controller. In: *OCEANS 2015-Genova* (pp 1–10). IEEE.

Skogestad, S., & Postlethwaite, I. (2007). *Multivariable feedback control: Analysis and design* (Vol. 2). New York: Wiley.

SNAME, T. (1950). Nomenclature for treating the motion of a submerged body through a fluid. The Society of Naval Architects and Marine Engineers, Technical and Research Bulletin, pp. 1–5.

Wirtensohn, S., Reuter, J., Blaich, M., Schuster, M., & Hamburger, O. (2013). Modelling and identification of a twin hull-based autonomous surface craft. In: *2013 18th international conference on methods and models in automation and robotics (MMAR)* (pp 121–126). IEEE.

Wu, F. (1995). Control of linear parameter varying systems. Ph.D. thesis, University of California at Berkeley, Grenoble.

Wu, F., Yang, X. H., Packard, A., & Becker, G. (1996). Induced l2-norm control for lpv systems with bounded parameter variation rates. *International Journal of Robust and Nonlinear Control*, *6*(9–10), 983–998.

Xiong, J., He, Y., Gu, F., Li, D., & Han, J. (2014). Quasi-lpv modeling and identification for a water-jet propulsion usv: An experimental study. In: *2014 IEEE international conference on robotics and biomimetics (ROBIO 2014)* (pp. 431–436). IEEE

Zhou, K., & Doyle, J. C. (1998). *Essentials of robust control* (Vol. 104). Upper Saddle River, NJ: Prentice Hall.